Performance Improvement of AlN–GaN-Based Intersubband Detectors by Using Quantum Dots

Daniel Hofstetter, Joab Di Francesco, Prem K. Kandaswamy, Aparna Das, Sirona Valdueza-Felip, and Eva Monroy

***Abstract*—We report a strong performance improvement for 1.55-μm AlN–GaN-based intersubband photodetectors. Thanks to the use of quantum dots (QDs) instead of quantum wells (QWs), a factor of 60 could be gained in terms of maximum responsivity. In addition, this performance was achieved at a considerably higher temperature of 160 K instead of 80 K as typically seen for QWs. The responsivity of these photodetectors, which are based on optical rectification, is strongly influenced by their excited state lifetime. We believe that a much longer electron lifetime in the upper QD states and an increased lateral electron displacement are responsible for the observed improvement.**

***Index Terms*—Photodetectors, quantum dots (QDs), semiconductors.**

I. Introduction

RESEARCH on mid- and near-infrared (IR) absorption via intersubband (ISB) transitions in AlN–GaN-based quantum wells (QWs) was initiated by Suzuki at Toshiba Corporation in 1999 [1]. For a couple of years, absorption experiments approaching the technologically relevant wavelength range around 1.55 μm were the only progress in this domain. Starting in 2003, AlN–GaN-based photodetectors for 1.55 μm became available [2], [3], and nitride ISB technology experienced increasing attention in research. Most recent milestones in this area include the demonstration of high-frequency detection [4], the successful operation of quantum cascade detectors [5], and the discovery of optical rectification in such structures [6]. One important point, however, could not be clarified until recently: Some of the early devices showed a surprisingly high room-temperature response, a feature which could not systematically be reproduced until late 2008 [7]. Temperature-dependent analysis of these new structures including lateral conductivity, photoluminescence (PL), absorption, and response measurements allowed us to verify now the important role of the QW morphology. More specifically, our recent experiments reveal that the responsivity of detectors having nanostructured quantum-dot (QD)-like active regions offer nearly two orders of magnitude higher responsivities than their QW-like counterparts. Since QWs for nitride-based near-IR devices are as thin as 5 to 6 monolayers (MLs), interface roughness can introduce significant in-plane carrier localization, which is enhanced by the polarization-induced internal electric field in these materials. Therefore, the difference between nitride-based QWs and QDs is not as well defined as in other material systems, and needs to be analyzed carefully. In this letter, we thus start with a general characterization of QW and QD active regions, and then present a comparison between QW-based and QD-based AlN–GaN ISB photodetectors. Given the operating mechanism of such devices (nonlinear optical rectification), the longer electron lifetime and the larger lateral displacement present in QDs are responsible for the marked performance improvement seen in the QD samples [8].

Manuscript received February 08, 2010; revised April 03, 2010; accepted May 02, 2010. Date of publication May 18, 2010; date of current version June 30, 2010. This work was initiated by the Gebert-Rüf-Stiftung, Basel, Switzerland and by armasuisse, Thun, Switzerland.

D. Hofstetter and J. Di Francesco are with the Institute of Physics, University of Neuchatel, 2009 Neuchatel, Switzerland (e-mail: Daniel.Hofstetter@unine.ch).

P. K. Kandaswamy, A. Das, S. Valdueza-Felip, and E. Monroy are with CEA Grenoble, 38054 Grenoble, France.

Color versions of one or more of the figures in this letter are available online at http://ieeexplore.ieee.org.

Digital Object Identifier 10.1109/LPT.2010.2050057

II. Fabrication/Experiments

In order to make a fair comparison, we fabricated two detector devices coming from the same growth batch. Except for the active region, which was QW-based in one case and QD-based in the other, all layer thicknesses and doping levels were identical. Epitaxial growth of the detector layers was based on plasma-assisted molecular-beam epitaxy on 1-μm-thick AlN-on-sapphire substrates. On top of this first AlN layer, we grew a 500-nm-thick AlN buffer followed by a 40 period active region, and a 100-nm-thick AlN cap layer. The active region was either a superlattice consisting of 1.5-nm-thick n-doped ($[\mathrm{Si}] = 2 \times 10^{19}$ cm^{-3}) GaN QWs separated by 5-nm-thick undoped AlN barrier layers, or a superlattice with GaN QDs resulting from N-rich deposition of 4 ML of n-doped ($[\mathrm{Si}] = 2 \times 10^{19}$ cm^{-3}) GaN and being separated by 5-nm-thick undoped AlN barriers. Transmission electron microscopy characterization on QD samples synthesized under exactly identical growth conditions as here revealed indeed a wetting layer thickness of roughly 2 ML, a QD height on the order of 1 nm, and a lateral dot size of about 4–6 nm [9]. The density of such truncated hexagonal dots was on the order of $1 - 2 \times 10^{12}$ cm^{-2}, resulting in a carrier density of roughly two electrons per QD. In contrast, typical QW samples have smooth layers with an interfacial roughness at the ML scale [10].

After growth, the samples were prepared as multipass zigzag waveguides (3.2 mm long for the QWs, 2.0 mm long for the QDs) with a polished back and two parallel polished faces at angles of 45° to the surface normal. This configuration allows efficient coupling of the incoming light into the waveguide, enables a good interaction between the ISB transition and the radiation, and offers equal Fresnel losses for both TE and TM polarization. Thermal evaporation of stripe-shaped Ti–Au (10/400 nm) contacts running perpendicularly to the 45° facet mirrors and having a dimension of 0.8×3 mm^2 completed device processing. Typical device geometry can be seen in [7]. The finished samples were then glued on copper heatsinks and

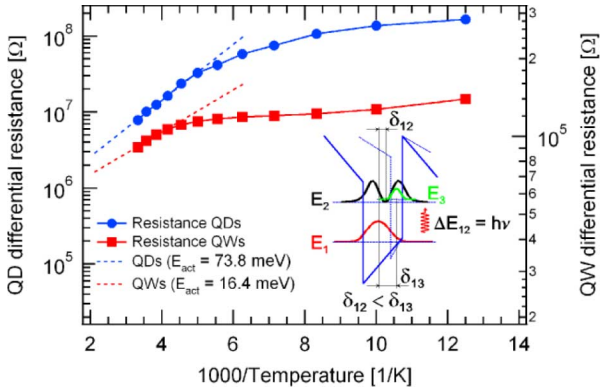

Fig. 1. Arrhenius plots of the differential resistance values around 0 V. By taking into account temperatures >200 K only, activation energies of 16.4 and 73.8 meV were found for the QW and the QD samples, respectively. The inset shows a simulated band structure of the QD sample (solid: QD, dotted: wetting layer) with the three lowest electronic states.

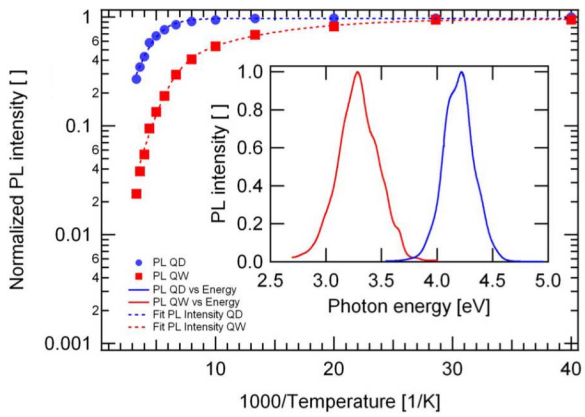

Fig. 2. Thermal evolution of the PL intensity of typical QW and QD samples. Solid lines are fits to (1), yielding activation energies of 17 and 102 meV for the QWs and about 79 meV for the QDs. The inset shows normalized PL spectra at 7 K for both samples.

wire bonded for electrical characterization. During the measurements, the detectors were placed in a liquid nitrogen-flow cryostat. Illumination was done using the internal white light source of a Fourier transform infrared (FTIR) spectrometer (Bruker AFS-66), while the produced detector signals were amplified with a voltage preamplifier (EG&G Instruments Model 5113) and fed back into the external detector port of the FTIR.

The simulated band structure of one active region period of the QD sample is shown in the inset of Fig. 1. Between the s state (E_1) and the p_z state (E_2), a transition energy of 870 meV and a dipole matrix element of 2.5 Å are predicted [11]. From level E_2, coupling to the ground state of the wetting layer, E_3, is possible. Since the probability of resonant tunneling across 5-nm-thick AlN barriers is very small, *no electron transport through the barriers* takes place. However, as in an asymmetric QW configuration, excitation of an electron into the p_z state or the wetting layer ground state is accompanied by an electron displacement in growth direction. Thanks to the small thickness of the wetting layer, this displacement is roughly 5–10 times larger than in a QW, namely about 10 Å. This confirms optical rectification as a detector mechanism of these photovoltaic devices [6]. Fig. 1 shows an Arrhenius plot of the differential resistance around 0 V and measured in lateral direction along the QW/QD layers. For temperatures between 200 K and 300 K, the QW differential resistance presents a thermal activation energy of $E_a^{\mathrm{QW}} = 16.4$ meV, while the QD curve shows a considerably higher value of $E_a^{\mathrm{QD}} = 73.8$ meV.

In order to further assess the different carrier confinement in the samples, temperature-dependent continuous-wave PL experiments using a frequency-doubled Argon laser emitting at 244 nm were performed. Fig. 2 shows the logarithmic signal intensity versus inverse temperature. While the QW sample has a constant intensity up to 30 K only, the QD sample's PL is nearly constant up to temperatures on the order of 160 K. The improved thermal stability of the QD PL signal is due to three-dimensional carrier localization in the dots, which hinders the electrons from moving towards nonradiative recombination centers [12]. In order to quantify the energetic barrier that the electrons need to surmount to reach the nonradiative recombination centers, we can apply the following equation [13]:

$$I(T) = I_0 \Big/ \left[\left(1 + a_1 \exp \frac{-E_{a1}}{kT}\right) \left(1 + a_2 \exp \frac{-E_{a2}}{kT}\right) \right] \tag{1}$$

where $I(T)$ is the PL intensity as a function of temperature, I_0 the PL intensity at 0 K, E_{a1} and E_{a2} are the activation energies involved in the carrier escape, a_1 and a_2 are fitting constants, and k is Boltzmann constant. This general equation assumes two nonradiative recombination paths that are related, the electron confinement being estimated from the lower activation energy. Fig. 2 presents the fit of the thermal evolution of the PL intensity of QWs and QDs to (1). Thermal activation energies of 17 ± 2 meV and 79 ± 5 meV were extracted for the QWs and QDs, respectively. These values are in good agreement to the ones found from the above-described transport measurements. The inset of Fig. 2 shows a comparison between the PL spectra of QWs and QDs. Since the density of states of the zero-dimensional QDs is much smaller than the one of the two-dimensional wetting layer, all levels in the QD ground state will be occupied. In the PL spectrum, this leads to radiative recombination between excited states at a much higher PL energy. In particular, the formula $E_{\mathrm{PL}}^{\mathrm{QD}} = E_{\mathrm{PL}}^{\mathrm{QW}} + E_{\mathrm{ISB}}^{\mathrm{QD}}$ applies, where $E_{\mathrm{PL}}^{\mathrm{QD}} = 4.2$ eV, $E_{\mathrm{PL}}^{\mathrm{QW}} = 3.25$ eV, and $E_{\mathrm{ISB}}^{\mathrm{QD}} = 0.895$ eV. The missing 55 meV in this equation can be explained via a slightly smaller thickness of the QDs with respect to the QWs. According to this, a slightly shorter ISB transition wavelength is expected for the QDs than for the QWs.

III. Results

Multipass (eight and five passes through QW and QD, respectively) TM-polarized absorption curves were measured from 100 K to 300 K for both the QW and QD samples. Due to the small electron density per QD, only the s ground level is populated. Therefore, the absorption lines are attributed to transition between the two first electron confined states in the QWs ($E_1 \rightarrow E_2$) and to transition from the s ground level of the QD to the first excited level along the growth axis, p_z. Although the oscillator strength for the QD transition is only approximately known, we used Fermi's golden rule to confirm that the observed absorption peak strengths of 12% for the QDs and 19% for the QWs along with the full-width at half-maximum (FWHM) cited below corresponded indeed to doping levels on

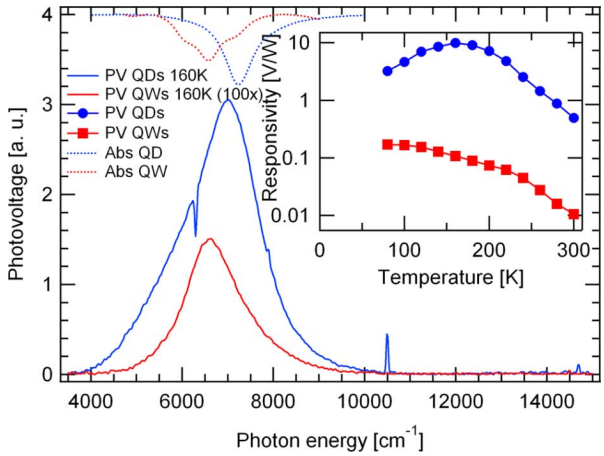

Fig. 3. Comparison between the spectral response and absorption curves (in a.u.) of the QD sample and the QW sample $(100\times)$ at 160 K. The responsivity spectra of the QD sample had to be corrected according to the formula $R_{\rm cor} = R_{\rm meas} \times \{(R_{\rm diff} + Z_{\rm in})/Z_{\rm in}\}$, where $Z_{\rm in} = 100\ M\Omega$ is the input impedance of the amplifier, $R_{\rm diff}$ the differential resistance of the device, $R_{\rm meas}$ the measured, and $R_{\rm cor}$ the corrected responsivity. The inset shows the corrected peak responses of QWs (red) and QDs (blue) as a function of temperature.

the order of 1.6×10^{19} cm^{-3} for the QWs and 2.5×10^{19} cm^{-3} for the QDs. The peak absorption—shown from the top x-axis of Fig. 3—is at 7220 cm^{-1} (1.39 μm, 895 meV) for the QD (FWHM = 760 cm^{-1}, 94 meV) and 6560 cm^{-1} (1.52 μm, 813 meV) for the QW sample (FWHM = 1150 cm^{-1}, 142 meV). These numbers confirm our prediction from PL.

Finally, we present in Fig. 3 the spectral response of both types of detectors. The spectral peak position and FWHM of the QW response are 6700 cm^{-1} (1.49 μm, 830 meV) and 1500 cm^{-1} (185 meV), respectively. In contrast, the QD sample peaks at 7000 cm^{-1} (870 meV, 1.43 μm) with an FWHM of 1800 cm^{-1} (223 meV). The inset shows normalized peak response versus temperature curves for both QW and QD detectors. For the QWs, the maximum response of 0.17 V/W is reached at 80 K, and the signal drops by more than one order of magnitude from 80 K to room temperature. In contrast, the QD sample reaches its maximum responsivity of 10 V/W at a considerably higher temperature, namely at 160 K. According to (1) in [6], this performance improvement can be explained by both a longer carrier lifetime in the excited quantum state and a larger lateral electron displacement, δ_{13}. With an estimated increase of 5–10 in lateral displacement due to the small wetting layer thickness and a lifetime increase of 5–10 due to the higher density of states in the wetting layer, we expect an overall responsivity improvement of 25–100. This agrees well with the observed factor of 60. Band structure calculations have indeed shown that strong coupling between the ground state of the QD wetting layer and the resonantly aligned p_z state plays an important role for both carrier lifetime (higher density of states in the wetting layer) and electron displacement. Finally, other effects such as carrier trapping in barrier layer defects might contribute to the long lifetime as well [14]. Further experiments will be necessary to clarify the role of the different mechanisms.

IV. Conclusion

We have presented a detailed study on nitride-based QW/QD samples used for photovoltaic ISB photodetection at 1.55 μm. Both lateral conduction and PL measurements confirmed that we have indeed fabricated two different samples having either QWs or QDs in the active region. Various effects such as a stronger localization of electrons in QDs, coupling of the p_z state to the ground state of the wetting layer, and a higher density of states in the latter result in a considerably higher maximum responsivity of the QDs with respect to the QWs. Although the somewhat longer carrier lifetime might have a detrimental effect on the detector speed, 100-GHz operation is still a realistic goal for such devices.

References

[1] N. Suzuki and N. Iizuka, "Effect of polarization field on intersubband transition in AlGaN/GaN quantum wells," *Jpn. J. Appl. Phys.*, vol. 38, pp. L363–L365, 1999.

[2] D. Hofstetter, S.-S. Schad, H. Wu, W. J. Schaff, and L. F. Eastman, "GaN/AlN-based quantum well infrared photodetector for 1.55 μm," *Appl. Phys. Lett.*, vol. 83, pp. 572–574, 2003.

[3] D. Hofstetter, E. Baumann, F. R. Giorgetta, M. Graf, M. Maier, F. Guillot, E. Bellet-Amalric, and E. Monroy, "High-quality AlN/GaN-superlattice structures for the fabrication of narrow-band 1.4 μm photovoltaic intersubband detectors," *Appl. Phys. Lett.*, vol. 88, no. 121112, 2006.

[4] F. R. Giorgetta, E. Baumann, F. Guillot, E. Monroy, and D. Hofstetter, "High frequency ($f = 2.37$ GHz) room temperature operation of 1.55 μm AlN/GaN-based intersubband detector," *Electron. Lett.*, vol. 43, pp. 185–187, 2007.

[5] A. Vardi, N. Kheirodin, L. Nevou, H. Machhadani, L. Vivien, P. Crozat, M. Tchernycheva, R. Colombelli, F. H. Julien, F. Guillot, C. Bougerol, E. Monroy, S. Schacham, and G. Bahir, "High-speed operation of GaN/AlGaN quantum cascade detectors at $\lambda = 1.55\ \mu$m," *Appl. Phys. Lett.*, vol. 93, no. 193509, 2008.

[6] D. Hofstetter, E. Baumann, F. R. Giorgetta, F. Guillot, S. Leconte, and E. Monroy, "Optically nonlinear effects in intersubband transitions of GaN/AlN-based superlattice structures," *Appl. Phys. Lett.*, vol. 91, no. 131115, 2007.

[7] D. Hofstetter, E. Baumann, F. R. Giorgetta, R. Théron, H. Wu, W. J. Schaff, J. Dawlaty, P. A. George, L. F. Eastman, F. Rana, P. K. Kandaswamy, S. Leconte, and E. Monroy, "Photodetectors based on intersubband transitions using III-nitride superlattice structures," *J. Phys., Condensed Matter*, vol. 21, no. 174208, 2009.

[8] H. Frohlich and T. K. Mitra, "Superconductivity in metals with incomplete inner shells," *J. Phys. C, Solid State Phys.*, vol. 1, pp. 544–548, 1968.

[9] F. Guillot, E. Bellet-Amalric, E. Monroy, M. Tchernycheva, L. Nevou, L. Doyennette, F. H. Julien, L. S. Dang, T. Remmele, M. Albrecht, T. Shibata, and M. Tanaka, "Si-doped GaN/AlN quantum dot superlattices for optoelectronics at telecommunication wavelengths," *J. Appl. Phys.*, vol. 100, no. 044326, 2006.

[10] P. K. Kandaswamy, F. Guillot, E. Bellet-Amalric, E. Monroy, L. Nevou, M. Tchernycheva, A. Michon, F. H. Julien, E. Baumann, F. R. Giorgetta, D. Hofstetter, T. Remmele, M. Albrecht, S. Birner, and L. S. Dang, "GaN/AlN short-period superlattices for intersubband optoelectronics: A systematic study of their epitaxial growth, design, and performance," *J. Appl. Phys.*, vol. 104, no. 093501, 2008.

[11] M. Tchernycheva, L. Nevou, L. Doyennette, F. H. Julien, and E. Warde, "Systematic experimental and theoretical investigation of intersubband absorption in GaN/AlN quantum wells," *Phys. Rev. B*, vol. 73, no. 125347, 2006.

[12] J. Renard, P. K. Kandaswamy, E. Monroy, and J. Gayral, "Suppression of nonradiative processes in long-lived polar GaN/AlN quantum dots," *Appl. Phys. Lett.*, vol. 95, no. 131903, 2009.

[13] M. Leroux, N. Grandjean, B. Beaumont, G. Nataf, F. Semond, J. Massies, and P. Gibart, "Temperature-quenching of photoluminescence intensities in undoped and doped GaN," *J. Appl. Phys.*, vol. 86, pp. 3721–3728, 1999.

[14] L. Nevou, J. Mangeney, M. Tchernycheva, F. H. Julien, F. Guillot, and E. Monroy, "Ultrafast relaxation and optical saturation of intraband AlN quantum dots," *Appl. Phys. Lett.*, vol. 94, no. 132104, 2009.